analytical chemistry

Article

Cite This: Anal. Chem. XXXX, XXX, XXX−XXX

pubs.acs.org/ac

Fenobody: A Ferritin-Displayed Nanobody with High Apparent Affinity and Half-Life Extension

Kelong Fan,*[,†,§] Bing Jiang,[†,‡,§] Zhe Guan,[∥] Jiuyang He,[†,‡] Dongling Yang,[†] Ni Xie,[⊥] Guohui Nie,[⊥] Can Xie,*[,∥] and Xiyun Yan*[,†,‡]

[†]Key Laboratory of Protein and Peptide Pharmaceuticals, CAS-University of Tokyo Joint Laboratory of Structural Virology and Immunology, Institute of Biophysics, Chinese Academy of Sciences, Beijing 100101, China

[‡]University of Chinese Academy of Sciences, 19A Yuquan Road, Beijing 100049, China

[∥]State Key Laboratory of Membrane Biology, Laboratory of Molecular Biophysics, School of Life Sciences, Peking University, Beijing 100871, China

[⊥]Institute of Translation Medicine, Shenzhen Second People's Hospital, First Affiliated Hospital of Shenzhen University, Shenzhen, 518035, China

Supporting Information

ABSTRACT: Nanobodies consist of a single domain variable fragment of a camelid heavy-chain antibody. Nanobodies have potential applications in biomedical fields because of their simple production procedures and low cost. Occasionally, nanobody clones of interest exhibit low affinities for their target antigens, which, together with their short half-life limit bioanalytical or therapeutic applications. Here, we developed a novel platform we named fenobody, in which a nanobody developed against H5N1 virus is displayed on the surface of ferritin in the form of a 24mer. We constructed a fenobody by substituting the fifth helix of ferritin with the nanobody. TEM analysis showed that nanobodies were displayed on the surface of ferritin in the form of 6 × 4 bundles, and that these clustered nanobodies are flexible for antigen binding in spatial structure. Comparing fenobodies with conventional nanobodies currently used revealed that the antigen binding apparent affinity of anti-H5N1 fenobody was dramatically increased (~360-fold). Crucially, their half-life extension in a murine model was 10-fold longer than anti-H5N1 nanobody. In addition, we found that our fenobodies are highly expressed in *Escherichia coli*, and are both soluble and thermo-stable nanocages that self-assemble as 24-polymers. In conclusion, our results demonstrate that fenobodies have unique advantages over currently available systems for apparent affinity enhancement and half-life extension of nanobodies. Our fenobody system presents a suitable platform for various large-scale biotechnological processes and should greatly facilitate the application of nanobody technology in these areas.

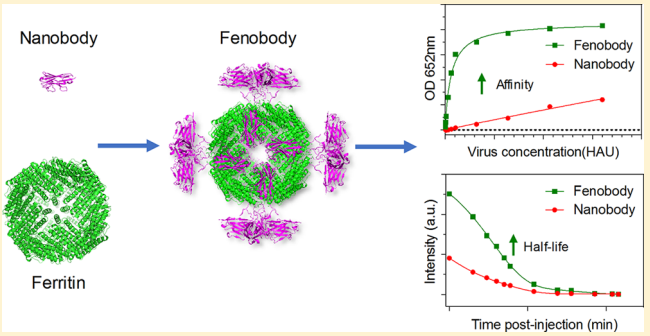

Nanobodies are comprised of a single domain variable fragment of a camelid heavy-chain antibody,[1] which was first reported in 1993.[2] Nanobodies (~15 kDa) are much smaller than intact conventional antibodies (~150 kDa) or fragments of antibodies [such as Fab (~50 kDa) and scFv (~25 kDa)].[3] Nanobodies are easily cloned through genetic engineering approach and robustly expressed in *Escherichia coli*, thereby offering an easy method to obtain large quantities of affinity-matured, antigen-specific antibodies.[4] The properties of nanobodies, such as simple production procedures, low cost, and high flexibility, allow them to be ideal candidates for diverse biomedical applications, including targeted drug delivery and therapy, disease diagnosis, bioimaging, and agricultural and plant protection.[5−12] To date, several nanobody drugs are being evaluated in clinical trials.[13]

The binding affinity of nanobodies to antigens isolated from nonimmune synthetic libraries is typically 10^2~10^3-fold lower than that of intact antibodies derived from immunized animals,[14,15] rendering nanobodies inadequate for bioanalytical applications requiring high sensitivity.[16] Several methods have been tested to increase the affinities of nanobodies, such as in vitro affinity maturation[17] and oligomerization.[16,18] Affinity maturation typically requires reconstructing library and rescreening for new nanobodies, all of which are time-consuming and expensive steps. Alternatively, oligomerization has been used to improve the affinity of nanobodies.[13,16,18−21] Different strategies to oligomerize nanobodies have been employed recently, namely, dimerization by linking nanobodies via soft linkers,[21] tetramerization by fusing nanobodies to streptavidin,[13] pentamerization by fusing nanobodies to verotoxin,[16,18] and

Received: December 14, 2017
Accepted: April 4, 2018
Published: April 4, 2018

DOI: 10.1021/acs.analchem.7b05217
Anal. Chem. XXXX, XXX, XXX−XXX

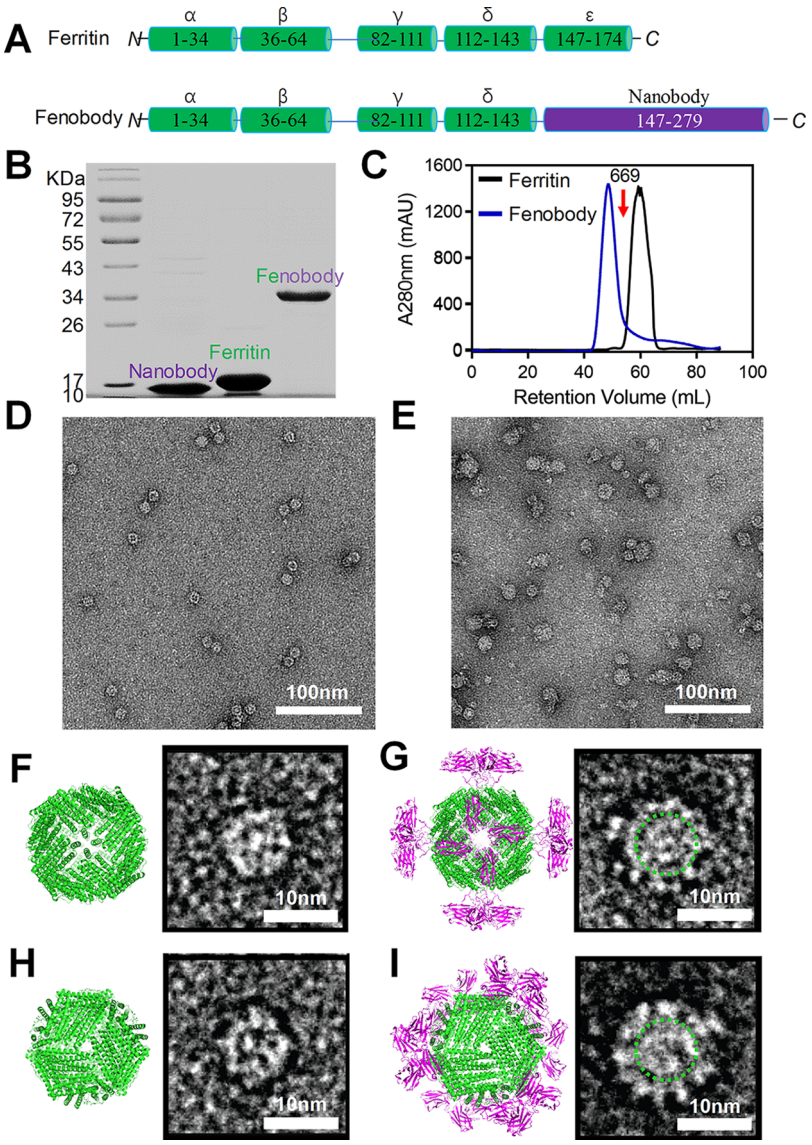

Figure 1. Characterization of fenobody architecture. (A) Structure of subunit of fenobody and ferritin. (B) SDS-PAGE analysis of subunit of fenobody, ferritin, and nanobody. (C) SEC analysis of self-assembled fenobody and ferritin. (D) TEM images of ferritin. (E) TEM images of fenobody. (F) Comparison between 3D structural models (left) and TEM images (right) of ferritin on the orientations of 4-fold symmetry axes. (G) Comparison between 3D structural models (left) and TEM images (right) of fenobody on the orientations of 4-fold symmetry axes. (H) Comparison between 3D structural models (left) and TEM images (right) of ferritin on the orientations of 3-fold symmetry axes. (I) Comparison between 3D structural models (left) and TEM images (right) of fenobody on the orientations of 3-fold symmetry axes. The 3D model of fenobody was prepared by PyMol based on the ferritin (PDB entry 2jd6) and nanobody structures (PDB entry 5e7b).

decamerization by fusing two types of nanobodies to the N-terminus and the C-terminus of verotoxin, respectively.[19] Therefore, oligomerization of nanobodies represents a promising approach to improve the binding affinity of nanobodies. Importantly, a novel molecular platform is required that is able to display polymerized nanobodies in correct orientation to maximize exposure of the antigen binding sites to antigens.

Due to the reduced size of nanobodies, they usually are rapidly excreted from the body, as shown by their short serum half-life. Short serum half-life might prevent optimum binding of nanobodies to the target molecule at tissues affected by a disease, resulting in reduced uptake compared with that of intact antibodies. Therapeutic applications typically require a slow drug clearance rate to avoid high dosage and frequent administration. Various approaches have been developed to extend the serum half-life of nanobodies in vivo, such as PEGylation or modification with a serum albumin-specific small chemical compound, genetic fusion with conformationally disordered polypeptides, or molecule binding to an abundant serum protein.[22] However, it was found that these modifications exhibit adverse effects on antibody functionality.[23] For instance, fusing nanobodies to albumin or immunoglobulin (Ig) fragment crystallizable region (Fc) decreases the yield of nanobodies in bacterial expression systems. Furthermore, fusion of nanobodies with IgG-specific nanobodies provokes Ig-mediated immune effector cell activation at undesired locations. Thus, methods that adversely affect the advantages of nanobodies are unsuitable for affinity enhancement and half-life extension of nanobodies.[4,7,22] Therefore, it is essential to develop strategies that both enhance the affinity and extend the half-life of nanobodies, thus allowing their effective use in nanobody-based applications for disease diagnosis and in vivo therapy.

DOI: 10.1021/acs.analchem.7b05217
Anal. Chem. XXXX, XXX, XXX−XXX

In this study, we chose ferritin as the basic structural framework and platform to display nanobodies. Ferritin is a spherical iron storage protein composed of a self-assembled 24-subunit protein shell with an outer diameter of 12 nm and interior cavity diameter of 8 nm.[24] Ferritin is easily produced in *E. coli* at high yield.[25] Due to its large numbers of salt bridges and hydrogen bonds, ferritin is extremely heat-resistant[24] and exhibits excellent biocompatibility in vivo.[26,27] The three-dimensional structure of ferritin is highly conserved from bacteria to mammals, with each of the 24 subunits typically consisting of a bundle of four long helices (α–δ), a fifth short helix (ε), and a long extended loop between β and γ helices (Figure 1A, upper panel).[28] Due to its ability to self-assemble and because of its unique architecture, ferritin has been used to display peptides[29−31] as well as larger proteins.[32−34] However, most previous studies constructed the fusion nanocages via inserting the exogenetic peptides or proteins at the N-terminus of the ferritin subunits, producing fusion proteins that are captured inside inclusion bodies, thus, dramatically reducing their yield.[29,30,33]

Using a rational design strategy, we employed ferritin from a hyper-thermophilic archaea *Pyrococcus furiosus* (living optimally at 100 °C[35]) as the structural framework to orient and display nanobodies on their surface and named this chimera protein fenobody.

RESULTS AND DISCUSSION

Fenobody Construction and Characterization. A broad spectrum anti-influenza A nanobody (16 kDa) was prepared in our previous work.[18] To produce fenobodies, we first genetically engineered ferritin (~18 kDa) by inserting the nanobody sequence at the C-terminus to substitute the ε helix of *P. furiosus* ferritin subunits (Figure 1A). The recombinant fenobodies were abundantly expressed in *E. coli* as soluble proteins (Figure S1A). As shown in Figure 1B, the purified fenobody subunits appear in a reduced SDS-PAGE as a single band of approximately 34 kDa, a molecular weight that is consistent with the theoretical size of the fusion protein. Size-exclusion chromatography (SEC) of ferritin and fenobody demonstrated that the recombinant fenobody exhibited a relatively larger hydrodynamic radius than that of ferritin (Figure 1C). After purification, both the ferritin and fenobody were analyzed by negative staining TEM. Both proteins showed globular shapes and resembled the cage-like architecture of ferritin (Figure 1D,E). The monodispersity of fenobody was confirmed by dynamic light scattering (DLS) analyses, and the sizes of the ferritin and fenobody were 13.99 ± 2.46 and 21.04 ± 4.47 nm, respectively (Figure S1B).

To investigate whether the nanobodies were successfully displayed on the outer surface of the recombinant nanocages, we analyzed the structural features of the negative stained ferritin and fenobody using TEM. We classified the TEM images of ferritin and fenobody into two types according to the orientation of 4-fold and 3-fold symmetry axes of the ferritin structure. For each type, representative TEM images were obtained. The structural features of each type are illustrated using a 3D model of ferritin and fenobody (Figure 1F−I). As shown in Figure 1G,I, the class 1 and class 2 TEM images of fenobody exhibited larger diameters and apparent protruding spikes than that of ferritin. In these figures, the size and boundary of the ferritin is labeled as green circles in both classes (right panel) to highlight the nanobodies, which are displayed on the surface. As shown in Figure 1G, apparent bundles of assembled nanobodies are present on the outer surface of fenobody. Based on this finding, we showed that during protein expression in *E. coli*, the fenobody subunits self-assembled into a nanocage. The 24 nanobodies were self-assembled as bundles in the 4-fold symmetry axes of the fenobody.

Fenobody Exhibit Thermal Stability. The heat-resistant (100 °C) properties of ferritin produced in *P. furiosus* have been reported previously.[35] Here, we tested the thermal stability of fenobody using a circular dichroism (CD) assay that measures changes in the spectrum as a function of temperature. As shown in Figure 2A, nanobody exhibited a typical CD spectra of β sheets, as a trough appeared at 216 nm wavelength signal, whereas fenobody exhibited typical CD spectra of α helices, as a trough appeared at 222 nm wavelength signal.

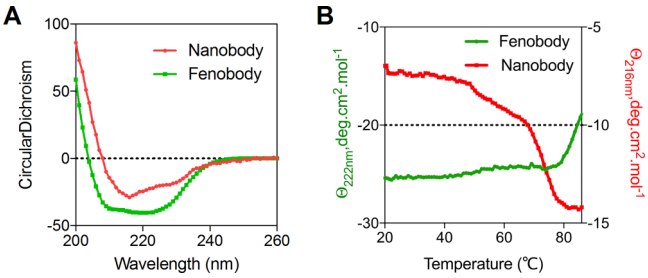

Figure 2. Thermal stability of fenobody analyzed by circular dichroism (CD). (A) CD spectra of fenobody and nanobody. (B) Thermal stability analysis of fenobody and nanobody. The half melting temperature (t_m value) of fenobody was higher than 80 °C, while that of nanobody was determined as 60 °C.

To monitor the thermal stability of nanobody and fenobody, we measured the 222 nm wavelength signal of fenobody and 216 nm wavelength signal of nanobody while increasing the temperature from 20 to 86 °C. Below 80 °C, we detected no visible changes in the CD spectrum of fenobody. In comparison, the CD spectrum of nanobody was dramatically changed. Above 80 °C, a sharp increase in signal intensity was visible in the CD spectrum of fenobody, presumably as a result of protein precipitation (Figure 2B). Together, these results demonstrated that our fenobodies are thermostable up to approximately 80 °C. Next, we compared these characteristics with those of currently existing nanobodies. We found that the t_m value of a typical nanobody is approximately 60 °C, which is consistent with other reports.[16] Thus, our results provide strong evidence that displaying nanobodies on the surface of ferritin significantly improves the thermal stability of nanobodies. The heat-stable property is necessary for antibody probes utilized for in vitro or some in vivo applications.[36] Thus, heat stability of our fenobodies is superior to antibody probes currently used.

Fenobody Exhibits High Affinity to H5N1 Virus. To test the specificity and binding affinity of fenobody to the H5N1 virus (A/Chicken/Henan/16/2004), we employed an ELISA-based method. Both fenobody and nanobody bound to the H5N1 virus, but the apparent affinity of our fenobody was 360× higher than that of a comparable nanobody structure. The original concentration (virus titer) of the H5N1 virus was 2^6 hemagglutination units (HAU)/mL, as determined using a standard HA test for influenza viruses. The binding of fenobody to the H5N1 virus antigens was saturable within 1 HAU/mL virus (Figure 3A).

To compare the binding affinity of fenobody with nanobody to the H5N1 virus, we calculated their K_d values using a saturation binding curve and Scatchard analysis. As shown in Figure 3A, the

DOI: 10.1021/acs.analchem.7b05217
Anal. Chem. XXXX, XXX, XXX−XXX

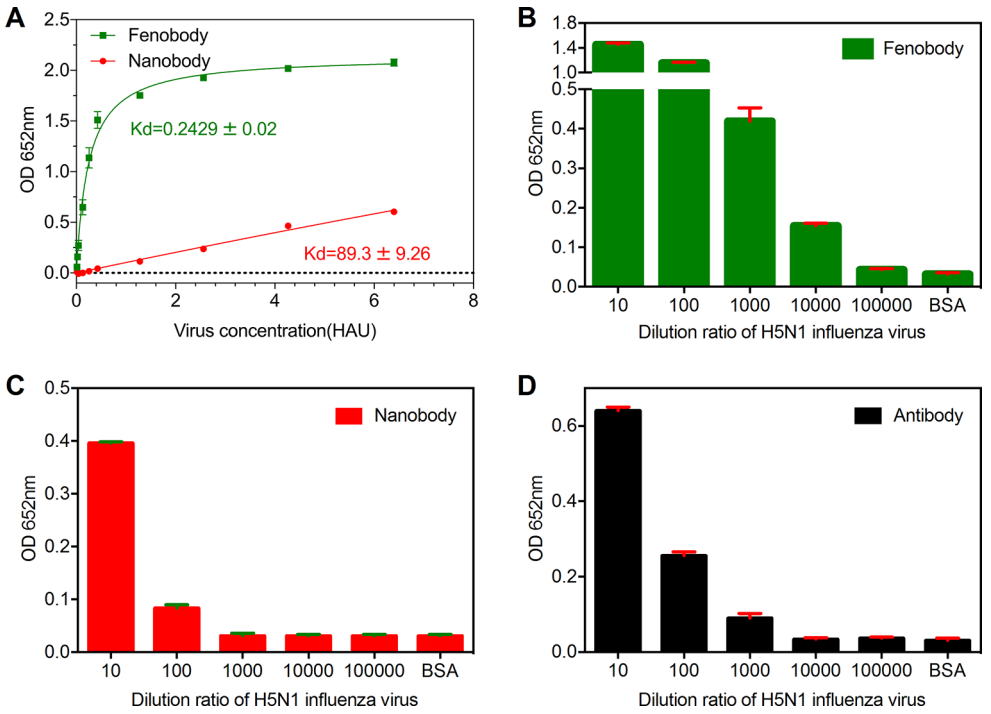

Figure 3. (A) Binding affinity analysis of fenobody and nanobody to H5N1 virus particles by ELISA. (B–D) Detect limit measurement of fenobody (B), nanobody (C), and antibody (D) to H5N1 virus particles by ELISA. The asterisk (*) indicates the limit of detection for H5N1 virus by ELISA methods.

K_d values of fenobody and nanobody to the H5N1 virus were 0.2429 ± 0.02 HAU/mL and 89.3 ± 9.26 HAU/mL, respectively (Figure 3A). Thus, displaying nanobodies on the surface of ferritin increased the apparent affinity of the nanobodies to the antigens by more than 360-fold.

Moreover, we demonstrated that even after the fenobody was treated for up to 60 min at 60 °C, its binding affinity to the H5N1 virus exhibited no significant change (Figure S2).

Fenobodies Exhibit High Sensitivity to H5N1 Virus. To explore whether fenobodies detect H5N1 virus with high sensitivity, we employed a double-antibody sandwich ELISA method. We used the same concentrations of fenobodies, nanobodies and commercial intact IgG antibodies as capture antibodies for ELISA to directly compare their sensitivity to virus detection. As shown in Figure 3B, the limit of detection (LOD) of the fenobody-based ELISA for the H5N1 virus was 10,000 times of diluted original H5N1 virus (A/Chicken/Henan/16/2004, 2^6 HAU/mL). In contrast, the LOD for nanobody was 100 times of diluted original H5N1 virus (Figure 3C), the LOD for antibody was 1,000 times of diluted original H5N1 virus (Figure 3D). In comparison, our BSA control yielded no specific binding. Together, these results indicated that a fenobody-based ELISA is 100-fold more sensitive than a nanobody-based ELISA, consistent with our results for the binding affinity analysis. Interestingly, a fenobody-based ELISA is 10-fold more sensitive than an antibody-based ELISA, indicating that fenobody is superior to intact antibody for virus detection.

Fenobodies Exhibit Half-Life Extension. Due to their tendency to oligomerize, the effective size and molecular weight of fenobodies is larger than nanobodies, which could theoretically extend its half-life. We performed animal experiments to determine the circulation half-life of fenobody in comparison with that of nanobody. We intravenously (*i.v.*) injected the identical doses of FITC-labeled fenobodies and FITC-labeled nanobodies into healthy mice, and studied the half-lives of fenobody and nanobody by analyzing the fluorescence values in the blood. As shown in Figure 4, both the fenobody and

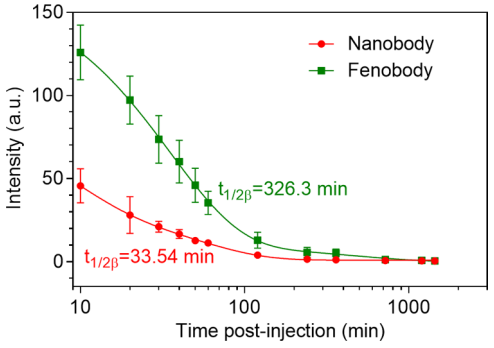

Figure 4. Plasma concentrations of fenobody and nanobody at different time points after intravenous injection into healthy mice.

nanobody showed biphasic plasma concentration profiles with a second phase $t_{1/2\beta}$ of 33.54 and 326.3 min, respectively (Figure 4, simulation performed with Kinetica software). The blood half-life of fenobody is nearly 10-fold higher compared to that of nanobodies, indicating that our fenobody is more suitable for in vivo applications.

CONCLUSIONS

In summary, we designed a novel nanobody display platform, named fenobody, based on ferritin. Fenobody was designed for improving binding affinity, increasing thermal resistance, and extending blood half-life in vivo of nanobody.

Oligomerization of nanobodies is a promising and quick way to improve the apparent affinity of nanobodies. Pentamerization of nanobodies was the highest multivalent of engineered nanobodies for the apparent affinity improvement to date.[13,16] In a previous study, we constructed pentamers of the same

DOI: 10.1021/acs.analchem.7b05217
Anal. Chem. XXXX, XXX, XXX−XXX

nanobodies used in this study, and we demonstrated that pentamerization of these nanobodies improved the binding affinity of the nanobodies to H5N1 virus by more than 5-fold.[18] Thus, displaying nanobodies on ferritin (24-mers) is more effective (more than 70-fold) improvement of binding affinity of nanobodies than that of pentamers of the nanobodies.

Moreover, the peptides/ligands display strategies employing ferritin as structural framework reported earlier are inserting the peptides/ligands to the N terminus of the ferritin subunit,[29,33] or the exposed loop region between helix δ and ε of the subunit,[30] or both sites.[37] This generally produces fusion proteins in inclusion bodies, resulting in reduced yield.[29,30,33] Also, the purification manipulations of fusion protein from inclusion bodies typically uses denaturants and reductants, which affect the avidity/affinity of final fusion proteins. Ferritin previously used are typically human HFn or LFn. The human HFn/LFn are less stable than *P. furiosus* ferritin.[35] Thus, the HFn/LFn based fusion proteins are typically unstable.

The excellent physical stability of the ferritin from *P. furiosus* allows the soluble expression of heat-stable fenobody in *E. coli* with high yield. Given that our fenobodies are far more heat stabile than their nanobody counterparts, they are ideally suited for scale-up experiments and translational studies.

In our previous study, the pentamerization of nanobodies based ELISA exhibited only comparable sensitivity with commercial antibody-based ELISA.[18] In comparison, here, our fenobody based ELISA was 10-fold more sensitive than that of the pentamer based ELISA. Thus, fenobody exhibits more advantage than pentamerization of nanobodies strategy.

In addition, after display on the surface of the ferritin, the nanobodies extended the blood half-life by nearly 10-fold in vivo. PEGylation or modification with a serum albumin-specific compound, and fusion with disordered polypeptides are typical strategies for improving the blood half-life of nanobodies in vivo, while these modifications also affect the functional properties of nanobodies.[4]

Another advantage of our fenobody system is that it can be customized by loading its 8 nm cavity with different reagents. For instance, by loading imaging dyes, together with the target function of nanobody, we may develop fenobody based tumor imaging. When loading near-infrared dyes,[38] we may further develop fenobody based imaging-guided photothermal therapy. By loading antidisease drugs, such as traditional chemotherapeutic drugs (doxorubicin, cisplatin),[39] our fenobody platform should be ideally suited for improved tumor therapy.

Compared to other approaches for oligomerized nanobody, for example, pentamerization generated by fusing nanobody to verotoxin, resulting in inevitable immune response and toxic effect,[19] our fenobodies are much safer in therapeutic applications. Ferritin is a highly conserved protein from prokaryote to mammal.[40] It typically exhibits low immunogenicity in biomedical applications.[41] However, the long-term/repeated use of fenobodies as therapeutics and their potential risks have not yet been investigated. Thus, systematic work is still required to study the biocompatibility of fenobodies in in vivo applications in the future.

Combining the advantages of affinity improvement, thermal resistance, and extended half-life in vivo, our fenobody is an ideal platform for improving the robustness and sensitivity of nanobodies-based disease diagnosis in vitro or improving the efficiency of nanobodies-based therapy in vivo.

EXPERIMENTAL PROCEDURES

Construction of the Fenobody Fusion Gene. The gene sequence encoding nanobody for the H5N1 virus was obtained from our previous work.[18] We constructed *P. furiosus* ferritin (ferritin)-nanobody by replacing the sequence encoding the helix ε and loop (147−174 aa) of the ferritin subunit with the nanobody sequence through a flexible amino acid linker (GGGSGGGGSGGGS). The gene sequence encoding fenobody with a Nde I site in the 5′ coding region and a BamH I site in the 3′coding region was synthesized by Genecreate Biological Engineering Co., Ltd. (Wuhan, China). The 840 bp gene sequence was subsequently cloned into the *E. coli* expression vector pET-15b plasmid (Novagen, Merck Biosciences, Germany) with the Nde1 and BamH1 restriction sites, thus, a His-tag was expressed at the N-terminus of subunit of fenobody as a fusion protein. After the plasmid vector was transformed into *E. coli* DH5α (TransGen Biotech, Beijing, China), positive colonies were selected by polymerase chain reaction (PCR) using T7 primers, and were grown overnight in LB medium containing 100 mg/L of ampicillin. The fenobody-pET-15b plasmid was isolated using a EasyPure Plasmid MiniPrep Kit (TransGen Biotech, China) and the inserted DNA was confirmed by DNA sequencing (Invitrogen, U.S.A.).

Preparation of Fenobody Nanoparticles. To produce fenobody nanoparticles, the expression vector fenobody-pET-15b was transformed into *E. coli* transetta (DE3) (TransGen Biotech, China) according to the manufacturer's instructions. The transformed *E. coli* were cultured in lysogeny broth (LB) medium. The fenobody protein was expressed in *E. coli* where it self-assembled into the 24 subunit nanocage. The transformed *E. coli* cells were grown overnight in LB medium with 100 mg/L of ampicillin at 37 °C. Then, fenobody protein production was induced by isopropyl-β-D-thiogalactoside (IPTG, 1 mM, Sigma-Aldrich, St. Louis, MO, U.S.A.), and cells were incubated for an additional 10 h at 25 °C. After incubation, the *E. coli* cells were harvested by centrifugation at 4000 g at 4 °C for 45 min and the pellets were resuspended in Tris buffer (20 mM Tris, pH 8.0).

The resuspended *E. coli* cells was disrupted by sonication on ice and centrifuged at 15,000 g at 4 °C for 30 min. Soluble fenobody containing His-tags was purified from the supernatant by immobilized metal affinity chromatography (IMAC) using a Ni-NTA-Sefinose Column (Sangon Biotech, Shanghai, China). The fenobody protein was eluted using 300 mM imidazole (Sigma-Aldrich, St. Louis, MO, U.S.A.) and subsequently dialyzed against phosphate buffer solution (PBS). Finally, the fenobody protein was purified by SEC on a Sepharose 6 PG XK 16/70 column (GE Healthcare, U.K.) in sodium chloride solution (0.1 M NaCl). The concentration of fenobody was determined in triplicate using the BCA Protein Assay Kit (Pierce, U.S.A.) with bovine serum albumin as the standard. The typical yield of fenobody was 50 mg per 1 L batch.

Biophysical Characterization of Nanobody, Ferritin, and Fenobody Nanoparticles. The prepared ferritin nanoparticles and fenobody protein nanoparticles were characterized using SEC, TEM, and DLS.

SEC. The SEC analyses were performed on a Superdex 200 column (GE Healthcare, U.K.) installed on a Waters 515 solvent delivery system (Waters, Milford, U.S.A.) equipped with an in-line radioactivity detector and a Waters UV2487 dual wavelength absorbance detector.

TEM. For protein shell observation, the ferritin protein and fenobody nanoparticle samples (20 μL, 0.25 mg/mL) were

DOI: 10.1021/acs.analchem.7b05217
Anal. Chem. XXXX, XXX, XXX−XXX

negatively stained with uranyl acetate for TEM (JEM-1400) observation.

DLS. The ferritin and fenobody protein samples (100 μL, 0.25 mg/mL) were prepared in PBS buffer. The DLS analysis was performed using DynaPro Titan with a temperature-controlled microsampler (Wyatt Technology, U.S.A.) at 25 °C.

CD Spectrum Analysis. The CD spectra of nanobody and fenobody were obtained on a Chirascan-plus CD Spectrometer (Applied Photophysics, U.K.) at 25 °C. Samples were resuspended in PBS and used at 0.25 mg/mL. The spectra were measured from 260 to 200 nm with 0.1 nm resolution in a quartz cell with a 1 cm path length. To determine the thermostability of fenobody, sample temperatures were increased gradually from 20 to 86 °C. Spectra of 222 nm were then continuously recorded with increasing temperatures. The average of four ellipticity values was used to plot the sigmoidal graph of ellipticity versus temperature. The t_m values were determined as the temperature corresponding to 50% protein being denatured.

ELISA. To test the binding capacity of the purified fenobody to the influenza virus H5N1, nanobody (VHH3B, prepared according to our previous report[18]), fenobody, nanobody, and rabbit anti-H5N1 monoclonal antibody (Sino Biological Inc., Clone ID: 89, Beijing, China) with the same molarity (0.03 μM) were coated onto 96-well microtiter plates in coating buffer and blocked with 5% skim milk powder (Yi Li, China) for 2 h at 37 °C. The coated plates were incubated with various dilutions of the inactivated H5N1 avian influenza virus [the A/Chicken/Henan/16/2004(H5N1), with a virus titer of 2^6 HAU/mL determined by the standard HA test,[42] was kindly provided by Prof. George Fu Gao, Institute of Microbiology, Chinese Academy of Sciences] for 1 h at 37 °C and, subsequently, with mouse anti-H5N1 monoclonal antibody (1:2000, Sino Biological Inc., Beijing, China) for 1 h at 37 °C, then incubated with peroxidase linked antimouse antibody (1:3000, GE Healthcare, U.K.) for 1.5 h at 37 °C. Each incubation was followed by four washes with PBST and one wash with PBS. Finally, TMB substrate was added, and Absorption measured at 652 nm. The detection limit for detecting H5N1 virus were determined based on a cutoff value (mean of the blank control + 2× standard deviation).[43] All the experiments were repeated for three times and data represent the means ± SD of triplicate determinations.

Labeling of Fenobody and Nanobody. The preparation of FITC-fenobody and FITC-nanobody followed Fisher et al.[44] In brief, 200 nM fluorescein isothiocyanate isomer I (FITC; Sigma-Aldrich, U.S.A.) was added to either 50 nM fenobody or nanobody solution in 1 mL of carbonate/bicarbonate buffer (100 mM carbonate, pH 9.0). The mixture was incubated at room temperature for 1 h, then purified with a PD MiniTrap G-25 column (GE Healthcare, U.K.). The FITC-conjugated fenobody was concentrated and the buffer was exchanged with PBS in a Vivaspin-4 Centrifugal Concentrator (MWCO 100 k Da, Sartorius, Germany), for FITC-nanobody, the buffer was exchanged in a 3 k Da cutoff Vivaspin-500 Centrifugal Concentrator (Sartorius, Germany). The dye concentrations of FITC-fenobody and FITC-nanobody were determined by UV−vis spectroscopy (Nanodrop 2000, Thermo Fisher Scientific, U.S.A.). Protein concentration was measured by the BCA Protein Assay Kit (Pierce, U.S.A.) using bovine serum albumin as the standard.

Half-Life Test. All animal studies were performed with the approval of the Chinese Academy of Sciences Institutional Animal Care and Use Committee. To determine the pharmacokinetics of fenobody and nanobody, FITC labeled fenobody and FITC labeled nanobody (the dose of FITC was 2 nmols/mouse in ether FITC-fenobody or FITC-nanobody) were intravenously injected into female BALB/c mice (n = 6 for each group) via the tail vein. At selected time points (10, 20, 30, 40, 50, 60, 120, 240, 360, 720, 1200, and 1440 min), 20 μL of blood was collected from the tail vein and diluted in PBS with heparin (1000 U/mL). FITC-protein in the blood sample was measured by previously reported methods. Briefly, the blood sample was centrifuged (2000 rpm, 15 min, 4 °C) and plasma was obtained. Then, 10 μL of diluted plasma was incubated in 20 μL of DMSO to ensure capture of the maximal fluorescent signal. The fluorescence of the FITC-protein was determined on a Varioskan Flash Spectral Scanning Multimode Reader (Thermo Fisher Scientific, U.S.A.) using excitation at 488 nm and emission at 525 nm. To correct for nonspecific background fluorescence, the fluorescence of blood samples from untreated mice was also determined.

■ ASSOCIATED CONTENT

Supporting Information

The Supporting Information is available free of charge on the ACS Publications website at DOI: 10.1021/acs.analchem.7b05217.

Figures S1 and S2 (PDF).

■ AUTHOR INFORMATION

Corresponding Authors

*E-mail: yanxy@ibp.ac.cn. Tel.: +86-10-64888583.
*E-mail: canxie@pku.edu.cn. Tel.: +86-10-62753901.
*E-mail: fankelong@ibp.ac.cn. Tel.: +86-10-64888256.

ORCID

Kelong Fan: 0000-0001-6285-1933
Xiyun Yan: 0000-0002-7290-352X

Author Contributions

§These authors contributed equally to this work.

Notes

The authors declare no competing financial interest.

■ ACKNOWLEDGMENTS

The authors would like to acknowledge Ruofei Zhang and Yaxin Hou for their assistance in protein purification experiments. This work was supported by the Beijing Natural Science Foundation (Grant No. 5164037), Key Research Program of Frontier Sciences, CAS (Grant No. QYZDB-SSW-SMC013), Young Elite Scientist Sponsorship Program by CAST (2015QNRC001), National Natural Science Foundation of China (Grant Nos. 31530026 and 81671810), Strategic Priority Research Program of the Chinese Academy of Sciences (Grant No. XDA09030306), China Postdoctoral Science Foundation (Grant No. 2015M570158), China Postdoctoral Science Special Foundation (Grant No. 2016T90143), and Sanming Project of Medicine in Shenzhen (SZSM201612031).

■ REFERENCES

(1) Cortez-Retamozo, V.; Backmann, N.; Senter, P. D.; Wernery, U.; De Baetselier, P.; Muyldermans, S.; Revets, H. *Cancer Res.* **2004**, *64*, 2853−2857.

(2) Hamerscasterman, C.; Atarhouch, T.; Muyldermans, S.; Robinson, G.; Hamers, C.; Songa, E. B.; Bendahman, N.; Hamers, R. *Nature* **1993**, *363*, 446−448.

(3) Chakravarty, R.; Goel, S.; Cai, W. *Theranostics* **2014**, *4*, 386−398.

DOI: 10.1021/acs.analchem.7b05217
Anal. Chem. XXXX, XXX, XXX−XXX

(4) Hassanzadeh-Ghassabeh, G.; Devoogdt, N.; De Pauw, P.; Vincke, C.; Muyldermans, S. *Nanomedicine* **2013**, *8*, 1013−1026.
(5) Kruwel, T.; Nevoltris, D.; Bode, J.; Dullin, C.; Baty, D.; Chames, P.; Alves, F. *Sci. Rep.* **2016**, *6*, 21834.
(6) Wang, Y.; Fan, Z.; Shao, L.; Kong, X.; Hou, X.; Tian, D.; Sun, Y.; Xiao, Y.; Yu, L. *Int. J. Nanomed.* **2016**, *11*, 3287−3303.
(7) Bruce, V. J.; McNaughton, B. R. *Anal. Chem.* **2017**, *89*, 3819−3823.
(8) Keyaerts, M.; Xavier, C.; Heemskerk, J.; Devoogdt, N.; Everaert, H.; Ackaert, C.; Vanhoeij, M.; Duhoux, F. P.; Gevaert, T.; Simon, P.; Schallier, D.; Fontaine, C.; Vaneycken, I.; Vanhove, C.; De Greve, J.; Lamote, J.; Caveliers, V.; Lahoutte, T. *J. Nucl. Med.* **2016**, *57*, 27−33.
(9) Chen, J.; He, Q. H.; Xu, Y.; Fu, J. H.; Li, Y. P.; Tu, Z.; Wang, D.; Shu, M.; Qiu, Y. L.; Yang, H. W.; Liu, Y. Y. *Talanta* **2016**, *147*, 523−530.
(10) Buchfellner, A.; Yurlova, L.; Nuske, S.; Scholz, A. M.; Bogner, J.; Ruf, B.; Zolghadr, K.; Drexler, S. E.; Drexler, G. A.; Girst, S.; Greubel, C.; Reindl, J.; Siebenwirth, C.; Romer, T.; Friedl, A. A.; Rothbauer, U. *PLoS One* **2016**, *11*, e0151041.
(11) Kijanka, M.; Dorresteijn, B.; Oliveira, S.; van Bergen en Henegouwen, P. M. *Nanomedicine (London, U. K.)* **2015**, *10*, 161−174.
(12) Talelli, M.; Oliveira, S.; Rijcken, C. J.; Pieters, E. H.; Etrych, T.; Ulbrich, K.; van Nostrum, R. C.; Storm, G.; Hennink, W. E.; Lammers, T. *Biomaterials* **2013**, *34*, 1255−1260.
(13) Nunez-Prado, N.; Compte, M.; Harwood, S.; Alvarez-Mendez, A.; Lykkemark, S.; Sanz, L.; Alvarez-Vallina, L. *Drug Discovery Today* **2015**, *20*, 588−594.
(14) Muyldermans, S.; Lauwereys, M. *J. Mol. Recognit.* **1999**, *12*, 131−140.
(15) Yau, K. Y. F.; Dubuc, G.; Li, S. H.; Hirama, T.; MacKenzie, C. R.; Jermutus, L.; Hall, J. C.; Tanha, J. *J. Immunol. Methods* **2005**, *297*, 213−224.
(16) Zhang, J.; Tanha, J.; Hirama, T.; Khieu, N. H.; To, R.; Tong-Sevinc, H.; Stone, E.; Brisson, J. R.; MacKenzie, C. R. *J. Mol. Biol.* **2004**, *335*, 49−56.
(17) Friedman, M.; Orlova, A.; Johansson, E.; Eriksson, T. L. J.; Hoiden-Guthenberg, I.; Tolmachev, V.; Nilsson, F. Y.; Stahl, S. *J. Mol. Biol.* **2008**, *376*, 1388−1402.
(18) Mu, B.; Huang, X.; Bu, P.; Zhuang, J.; Cheng, Z.; Feng, J.; Yang, D.; Dong, C.; Zhang, J.; Yan, X. *J. Virol. Methods* **2010**, *169*, 282−289.
(19) Stone, E.; Hirama, T.; Tanha, J.; Tong-Sevinc, H.; Li, S.; MacKenzie, C. R.; Zhang, J. *J. Immunol. Methods* **2007**, *318*, 88−94.
(20) Conrath, K. E.; Lauwereys, M.; Wyns, L.; Muyldermans, S. *J. Biol. Chem.* **2001**, *276*, 7346−7350.
(21) Peyvandi, F.; Callewaert, F. *N. Engl. J. Med.* **2016**, *374*, 2497−2498.
(22) Kontermann, R. E. *Curr. Opin. Biotechnol.* **2011**, *22*, 868−876.
(23) Kubetzko, S.; Sarkar, C. A.; Pluckthun, A. *Mol. Pharmacol.* **2005**, *68*, 1439−1454.
(24) Fan, K.; Gao, L.; Yan, X. *WIREs Nanomed. Nanobiotechnol.* **2013**, *5*, 287−298.
(25) Fan, K.; Cao, C.; Pan, Y.; Lu, D.; Yang, D.; Feng, J.; Song, L.; Liang, M.; Yan, X. *Nat. Nanotechnol.* **2012**, *7*, 459−464.
(26) Liang, M.; Fan, K.; Zhou, M.; Duan, D.; Zheng, J.; Yang, D.; Feng, J.; Yan, X. *Proc. Natl. Acad. Sci. U. S. A.* **2014**, *111*, 14900−14905.
(27) Zhao, Y.; Liang, M.; Li, X.; Fan, K.; Xiao, J.; Li, Y.; Shi, H.; Wang, F.; Choi, H. S.; Cheng, D.; Yan, X. *ACS Nano* **2016**, *10*, 4184−4191.
(28) Harrison, P. M.; Arosio, P. *Biochim. Biophys. Acta, Bioenerg.* **1996**, *1275*, 161−203.
(29) Uchida, M.; Flenniken, M. L.; Allen, M.; Willits, D. A.; Crowley, B. E.; Brumfield, S.; Willis, A. F.; Jackiw, L.; Jutila, M.; Young, M. J.; Douglas, T. *J. Am. Chem. Soc.* **2006**, *128*, 16626−16633.
(30) Jeon, J. O.; Kim, S.; Choi, E.; Shin, K.; Cha, K.; So, I. S.; Kim, S. J.; Jun, E.; Kim, D.; Ahn, H. J.; Lee, B. H.; Lee, S. H.; Kim, I. S. *ACS Nano* **2013**, *7*, 7462−7471.
(31) Ji, T.; Zhao, Y.; Wang, J.; Zheng, X.; Tian, Y.; Zhao, Y.; Nie, G. *Small* **2013**, *9*, 2427−2431.
(32) Li, K.; Zhang, Z. P.; Luo, M.; Yu, X.; Han, Y.; Wei, H. P.; Cui, Z. Q.; Zhang, X. E. *Nanoscale* **2012**, *4*, 188−193.
(33) Li, X.; Qiu, L. H.; Zhu, P.; Tao, X. Y.; Imanaka, T.; Zhao, J.; Huang, Y. G.; Tu, Y. P.; Cao, X. N. *Small* **2012**, *8*, 2505−2514.
(34) Kanekiyo, M.; Wei, C. J.; Yassine, H. M.; McTamney, P. M.; Boyington, J. C.; Whittle, J. R.; Rao, S. S.; Kong, W. P.; Wang, L.; Nabel, G. J. *Nature* **2013**, *499*, 102−106.
(35) Tatur, J.; Hagen, W. R.; Matias, P. M. *JBIC, J. Biol. Inorg. Chem.* **2007**, *12*, 615−630.
(36) Willuda, J.; Honegger, A.; Waibel, R.; Schubiger, P. A.; Stahel, R.; Zangemeister-Wittke, U.; Pluckthun, A. *Cancer Res.* **1999**, *59*, 5758−5767.
(37) Kim, S.; Jeon, J. O.; Jun, E.; Jee, J.; Jung, H. K.; Lee, B. H.; Kim, I. S.; Kim, S. *Biomacromolecules* **2016**, *17*, 1150−1159.
(38) Huang, P.; Rong, P. F.; Jin, A.; Yan, X. F.; Zhang, M. G.; Lin, J.; Hu, H.; Wang, Z.; Yue, X. Y.; Li, W. W.; Niu, G.; Zeng, W. B.; Wang, W.; Zhou, K. C.; Chen, X. Y. *Adv. Mater.* **2014**, *26*, 6401−6408.
(39) Belletti, D.; Pederzoli, F.; Forni, F.; Vandelli, M. A.; Tosi, G.; Ruozi, B. *Expert Opin. Drug Delivery* **2017**, *14*, 825−840.
(40) Truffi, M.; Fiandra, L.; Sorrentino, L.; Monieri, M.; Corsi, F.; Mazzucchelli, S. *Pharmacol. Res.* **2016**, *107*, 57−65.
(41) Wang, Z.; Gao, H.; Zhang, Y.; Liu, G.; Niu, G.; Chen, X. *Front. Chem. Sci. Eng.* **2017**, *11*, 633−646.
(42) Killian, M. L. *Methods Mol. Biol.* **2008**, *436*, 47−52.
(43) Duan, D. M.; Fan, K. L.; Zhang, D. X.; Tan, S. G.; Liang, M. F.; Liu, Y.; Zhang, J. L.; Zhang, P. H.; Liu, W.; Qiu, X. G.; Kobinger, G. P.; Gao, G. F.; Yan, X. Y. *Biosens. Bioelectron.* **2015**, *74*, 134−141.
(44) Fisher, J.; Devraj, K.; Ingram, J.; Slagle-Webb, B.; Madhankumar, A. B.; Liu, X.; Klinger, M.; Simpson, I. A.; Connor, J. R. *Am. J. Physiol. Cell. Physiol.* **2007**, *293*, C641−649.

DOI: 10.1021/acs.analchem.7b05217
Anal. Chem. XXXX, XXX, XXX−XXX